Available online at www.sciencedirect.com

SciVerse ScienceDirect

Ceramics International 39 (2013) 8311–8317

CERAMICS INTERNATIONAL

www.elsevier.com/locate/ceramint

# Morphology-controlled synthesis of $SnO_2$ nanostructures using hydrothermal method and their photocatalytic applications

Nasrin Talebian*, Farzaneh Jafarinezhad

*Department of Chemistry, Shahreza branch, Islamic Azad University, Razi Chemistry Research Centre, Women Research Council, 86145-311 Shahreza, Isfahan, Iran*

Received 6 January 2013; received in revised form 3 March 2013; accepted 23 March 2013
Available online 10 April 2013

**Abstract**

$SnO_2$ hierarchical architectures were synthesized by a surfactant-free hydrothermal synthesis route. The influence of hydrothermal temperature and treatment time on the final morphology of the nanomaterials was studied. The as-synthesized nanoparticles were characterized by X-ray powder diffraction (XRD), UV–vis spectroscopy, scanning electron microscopy (SEM) and adsorption isotherm measurement. Degradation of aniline, 4-nitroaniline and 2,4-dinitroaniline as model organic pollutants was studied in the presence and absence of ultraviolet radiation. The effects of experimental parameters including irradiation time, solution pH and organics structure on the degradability were studied. The photodegradation of the pollutants followed first-order kinetics. The influence of $SnO_2$ morphology on its photocatalytic activity was comparatively investigated. The $SnO_2$ flower-shaped catalysts showed higher activity compared with others suggesting that the morphology of the catalysts exerts a noticeable influence on their performances.


*Keywords:* $SnO_2$; Hydrothermal; Morphology; Aniline; Photodegradation

## 1. Introduction

Shape- and size-controlled dispersible inorganic nanocrystals such as metals, semiconductors, and metal oxides have attracted considerable interests because of both their unique material properties compared with their bulk counterparts, and their corresponding theoretical and practical applications in chemistry, physics, material science, biology, and medicine [1–3]. Relative to size control, morphology control is more demanding to achieve by means of classical chemical approaches [4]. As a n-type direct wide-band semiconductor ($E_g = 3.6$ eV at 300 K), $SnO_2$ is transparent in the visible light region and useful as optoelectronic devices [5], catalyst supports [6], transparent conducting electrodes [7], antireflective coatings [8], and a proto-type material for metal oxide sensors [9].

Recent studies show that the performance of $SnO_2$ in these applications mainly depends on its morphology and structural features. Accordingly, considerable effort has recently been devoted to synthesizing $SnO_2$ nanostructures with different morphologies, including $SnO_2$ octahedra, nanorods, nanowires, nanobelts, nanotubes, hollow spheres, and mesoporous structures [10–17]. Morphological control of $SnO_2$ nanostructures is of great significance due to the interesting size- and shape-dependent properties [18]. The morphology of $SnO_2$ was found to be dependent on the synthesis conditions. Various methods are adopted for the preparation of nanometer tin oxide include the gas phase methods [19–21], sol-gel methods [22–24], evaporative decomposition of solution [19,25], laser ablation technique [26], and wet chemical synthesis [27–29].

Among many preparative methods for well-defined structures, the hydrothermal method is widely used to prepare the nanostructural materials because of its simplicity, high efficiency, and low cost. The main characteristic of this process is the low or medium temperature used compared to the conventional processes. On the other hand, the nanostructure

*Corresponding author. Tel.: +98 321 329 2260; fax: +98 321 3232701.
*E-mail addresses:* nasrin_talebian@yahoo.com, talebian@iaush.ac.ir (N. Talebian).

0272-8842/$ - see front matter © 2013 Elsevier Ltd and Techna Group S.r.l. All rights reserved.
http://dx.doi.org/10.1016/j.ceramint.2013.03.101

morphologies are tuned by changing experimental parameters. It is known that the time–temperature history of the process has a strong influence on the crystal structure and morphology of nanostructured materials [30].

In the past two decades, advanced oxidation processes (AOPs) using semiconductor powders as photocatalysts have widely been employed to treat a variety of industrial wastewaters containing aromatic amines, phenols, dyes, pesticides, toxic and biologically refractory organic substances. Aniline and its derivatives are toxic chemicals present in the effluent of many industries as they are widely used as raw materials in the manufacturing of a number of products such as dyes, plastics, resins, pharmaceuticals, petro-chemicals, herbicides, and pesticides [31–33]. Aniline and its derivatives are considered to be a health risk due to their strong toxicity and mutagenicity [34]. To treat wastewaters and affected soils containing aniline and most of its derivatives, remedies often used are photodecomposition, auto-oxidation, electrolysis, resin adsorption or ozone oxidation and biological treatment [35–39].

Among aniline derivatives, *p*-nitroaniline (PNA) and 2,4-dinitroaniline (DNA) have been listed as priority pollutants by many countries due to their toxicity, potential carcinogenic and mutagenic effects. The presence of a nitro group in the aromatic ring enhances the stability to chemical and biological oxidation degradation [40]. Besides, the anaerobic degradation produces nitroso and hydroxylamines compounds which are known as carcinogenic [41,42]. So the purification of wastewater polluted with PNA and DAN is a very difficult task.

Tin oxide materials have been widely used as catalysts in chemical reactions. The catalytic activity of $SnO_2$ catalysts was carried using different morphologies towards CO oxidation [43], methanol and ethanol electrooxidation [44], $H_2$ evolution [45] and hydrogenation of esters [46]. There are a few reports on the comparative photocatalytic properties of inorganic semiconductors including $SnO_2$ single film and powder [47–50]. However, more studies have been conducted on the photocatalytic treatment of environmental pollutants using $SnO_2$-based nanocomposites [51–56]. To the best of our knowledge, there are no reports focused on the single $SnO_2$ catalytic activity especially toward morphology-dependant aniline derivatives photodegradation.

In this work, we have synthesized $SnO_2$ nanostructures by hydrothermal method without pre-addition of various surfactants and templates. We have also studied the influence of heating time and temperature on their structures and morphologies and catalytic activities toward aniline derivatives degradation. The results indicated that $SnO_2$ nanoflowers exhibited higher activities, suggesting that the morphology of the catalyst has exerted a noticeable influence on the catalytic performance.

## 2. Experimental

### 2.1. $SnO_2$ powder preparation

In a typical process, desired amount $SnCl_4 \cdot 5H_2O$ and 1.4 g NaOH were mixed with 40 ml de-ionized water under magnetic stirring for 10 min. Next, 40 ml absolute ethanol was dropped slowly into the solution to make the white precipitation. The mixture was stirred for 24 h and then the whole mixture was transferred into 150 ml Teflon-linked autoclave. The autoclave was placed in an oven under different reaction temperatures (170–190 °C) for different periods of time (4–48 hours) to react at temperature ($T$) for time ($t$). The detailed experimental scheme is shown in Table 1. After the reaction complete, the resulting solid product was filtered and washed several times by de-ionized water, absolute ethanol and finally dried at 120 °C in air for 24 h.

Table 1
Experimental parameters for synthesizing $SnO_2$ powders.

| Sample | Hydrothermal temperature (°C) | Treatment time (h) |
|---|---|---|
| A | 190 | 48 |
| B | 190 | 24 |
| C | 160 | 20 |
| D | 100 | 20 |

### 2.2. Characterization

The resulting hydrothermally synthesized $SnO_2$ powders were characterized by X-ray diffraction (XRD, Bruker, D8 ADVANCE with Cu Kα radiation), UV–vis spectrometery (Shimadzu, MPC-2200), scanning electron microscopy (SEM, Philips, XL30 scanning electron microscope) and nitrogen adsorption measurement (A-series BEL SORP 18).

### 2.3. Photocatalytic experiment

The photocatalytic activities of $SnO_2$ photocatalysts were evaluated by the degradation of aniline, 4-nitroaniline (PNA) and 2,4-dinitroaniline (DNA) as model organic pollutants. The suspensions for the photocatalytic reaction were prepared by adding 0.1 g of the various samples to a certain concentration of aniline solution. Prior to illumination, the suspensions were magnetically stirred in the dark for 30 min to ensure the establishment of adsorption–desorption equilibrium of organic compounds on the powder surfaces. The equilibrium adsorption degrees for all investigated samples were determined to be less than 3.0%. All experimental conditions were kept constant as following: 100 ml of the suspension, 20 mg/L of initial organic compound concentration, continuous magnetic stirring and illumination with four 8 W UV lamps (Philips UV-A, $\lambda = 350$ nm) as UV source. Samples (10 ml) were extracted through pipette every 20 min and centrifuged immediately for analysis. The decomposition of aniline, 4-nitroaniline and 2,4-dinitroaniline was followed by monitoring the UV absorption band at 280, 380 nm and 346 nm, respectively. Degradation efficiency, $D$, was calculated as $D = (A_0 - A)/A_0$, where $A_0$ and $A$ show initial absorbance and the sample absorbance after illumination at intervals, respectively. The activities of the as-prepared photocatalysts were evaluated by calculating the photodegradation efficiency of organic compounds

as a function of illumination time. Control experiment was carried out under the same condition, but without catalyst (photolysis).

## 3. Results and discussion

### 3.1. Structural properties

Typical XRD patterns of the samples were obtained in different hydrothermal conditions are shown in Fig. 1. The peak positions were matched well the standard data for $SnO_2$: JCPDS card no. 41-1445. No other crystalline byproducts were found in the pattern, indicating that the as-prepared samples had a pure rutile structure. This finding implied that the hydrothermal treating temperature and time are very important to obtain the pure phase $SnO_2$ with good crystallinity. The relative intensities of (101) and (110) peaks are the largest. The low index (110) face is the thermodynamically most-stable bulk termination in oxides with rutile structure [57–60] and has

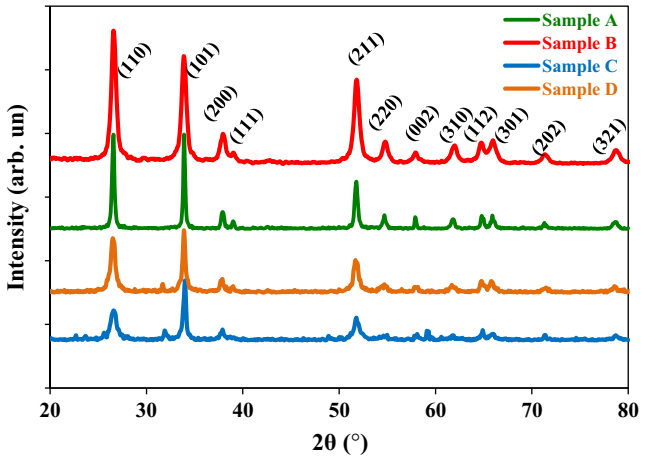


Fig. 1. The XRD patterns of the synthesized $SnO_2$ nanostructures after different times and temperatures.

the lowest surface energy [60–62]. The surface energies of $SnO_2$ follow the trend (110) < (100) < (101) < (001), indicating the *c*-axis to be the preferential growth direction [63]. By conducting experiments in solutions, the morphology is therefore dictated by the crystal symmetry as well as by the surface energy in the aqueous environment and thus the most stable crystal habit is directly generated without template or surfactant.

Further structural characterization of the $SnO_2$ powders was performed by SEM. It was found that the different hydrothermal treating temperatures and times lead to the different morphologies of samples including nano-flower (sample A, petal size: 120–280 nm diameter; 300–nm in length), nano-rod (sample B, 80–110 nm in diameter; 400 nm to 10 μm in length), nano-cauliflower (sample C, crystallite size: 70–105 nm) and micro-spherical (sample D, 0.4–1.8 μm diameter), as shown in SEM images (Fig. 2). The morphology of the final products may be explained by both crystal growth and nucleation theory in which the synthesis is separated into two steps: nucleation stage and crystal growth.

In the nucleation stage, $Sn(OH)_6^{2-}$ nucleus are created which decompose to $SnO_2$. Subsequently, $SnO_2$ crystalline particles grow along the (110) crystal direction and, thus, the possibility of synthesizing the rod-like and flower-like $SnO_2$ in the case of long enough treatment time and high temperatures is promising (samples A–C). At lower hydrothermal temperature (as for sample D) instead of crystal growth stage, the greater the number of nuclei was created in the solution where nuclei attracted species and other nuclei around them to form bigger micro-spherical ones.

### 3.2. Optical properties

UV/vis spectroscopy was used to characterize the optical adsorptions of $SnO_2$ samples. The fundamental absorption edge of the films corresponds to electron transitions from

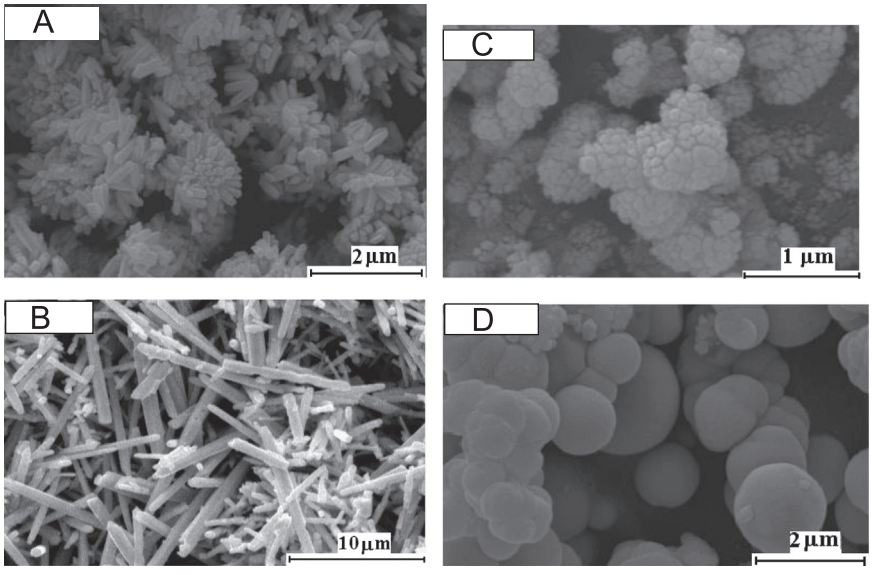


Fig. 2. SEM micrographs of $SnO_2$ samples.

valence band to conduction band and this edge can be used to calculate the optical band gap of the films. The optical transition of $SnO_2$ crystals is known to be a direct type [64]. In this case, the absorption coefficient $\alpha$ is expressed as $\alpha(h\upsilon) \propto (h\upsilon - E_g)^{1/2}/h\upsilon$ [65].

The band gap energies ($E_g$) were calculated on the basis of the corresponding absorption edges and by extrapolating the horizontal and sharply rising portions of the curve and defining the edge as the energy of the intersection (not shown here). $E_g$ values of $SnO_2$ powders varies from 3.44, 3.58, 3.51 and 3.79 eV for sample A, B, C and D, respectively.

As shown in Fig. 3, the absorption edge is red shifted for flower- and cauliflower- shape $SnO_2$ (Samples A and C) corresponds to decrease in their band-gap energy; the lower band-gap energy of a semiconductor results in an increase in photon harvesting and photo-responsive. Then, it is anticipated that samples A and C should show a higher photocatalytic activity than other samples.

### 3.3. Textural properties

Surface characterization of the $SnO_2$ samples was carried out from adsorption isotherms. In our samples, the surface areas increase in the order of sample A (88 $m^2/g$) > sample B (56 $m^2/g$) > sample C (51 $m^2/g$) > sample D (25 $m^2/g$).

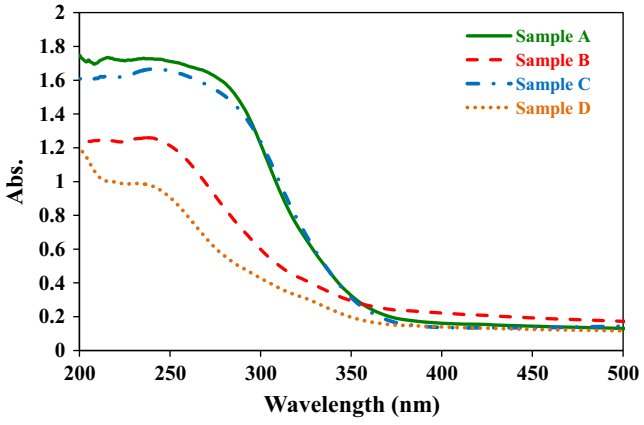


Fig. 3. UV–vis absorption spectra of the $SnO_2$ samples.

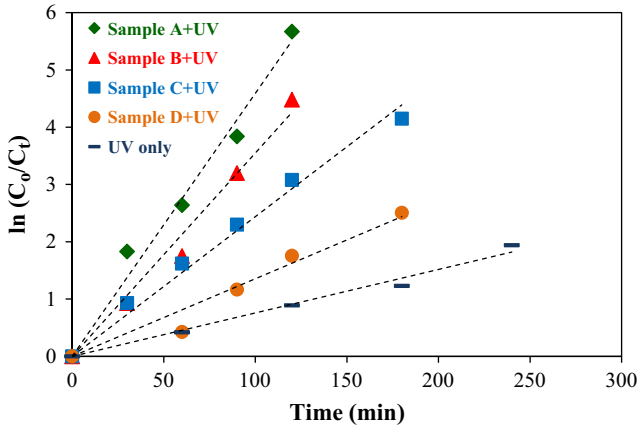


Fig. 4. Kinetics data of photocatalytic and pholytic degradation of aniline at pH=11.

### 3.4. Evaluation of photocatalytic activity

The catalytic activities of the samples were studied using, as a test reaction, the decomposition of the aniline compounds at room temperature. The UV–vis spectra of aniline, 4-nitroaniline and 2,4-dinitroaniline at different reaction times were recorded in the 600–200 nm wavelength range and showed main absorption bands at 280, 349 and 356 nm, respectively. These bands diminish gradually until they disappear, which indicates that the organic compounds photodecomposition is complete.

As seen in Figs. 4–6, the photoreactivity of sample A is superior to those of others and of all samples follows as sample A > sample C > sample B > sample D. Pseudo-first order photodegradation and photocatalytic kinetics were observed and the reaction constants were determined using Langmuir–Hinshelwood model and were reported in Table 2. The enhancement in the photocatalytic activity for flower-shape samples may be correlated to significantly higher absorbance

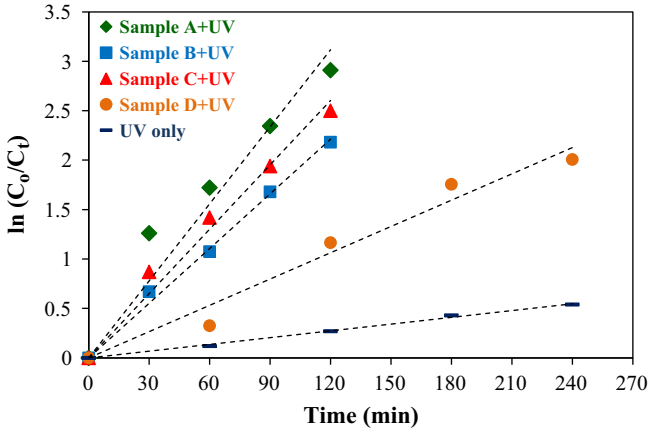


Fig. 5. Kinetics data of photocatalytic and pholytic degradation of PNA at pH=4.

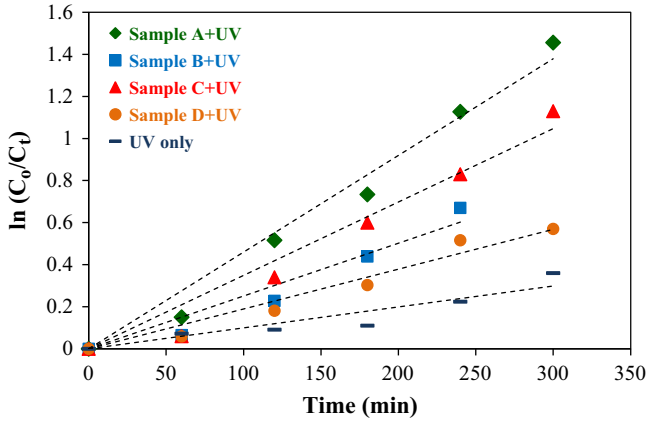


Fig. 6. Kinetics data of photocatalytic and pholytic degradation of DNA at pH=4.

Table 2
Influence of pH on the photocatalytic degradation of aniline compounds after 120 min UV illumination.

| Rate constants of photocatalyst ($min^{-1}$) | | | | | |
|---|---|---|---|---|---|
| pollutant | Sample A | Sample B | Sample C | Sample D | pH |
| Aniline | 0.0459 | 0.0244 | 0.0355 | 0.0135 | 4 |
| | 0.0561 | 0.0311 | 0.0439 | 0.0275 | 7 |
| | 0.0629 | 0.0453 | 0.0543 | 0.0343 | 10 |
| PNA | 0.0260 | 0.0184 | 0.0217 | 0.0089 | 4 |
| | 0.0201 | 0.0146 | 0.0182 | 0.0057 | 7 |
| | 0.0115 | 0.0061 | 0.0083 | 0.0018 | 10 |
| DNA | 0.0046 | 0.0025 | 0.0035 | 0.0019 | 4 |
| | 0.0028 | 0.0012 | 0.0018 | 0.0007 | 7 |
| | 0.0008 | 0.0004 | 0.0006 | 0.0004 | 10 |

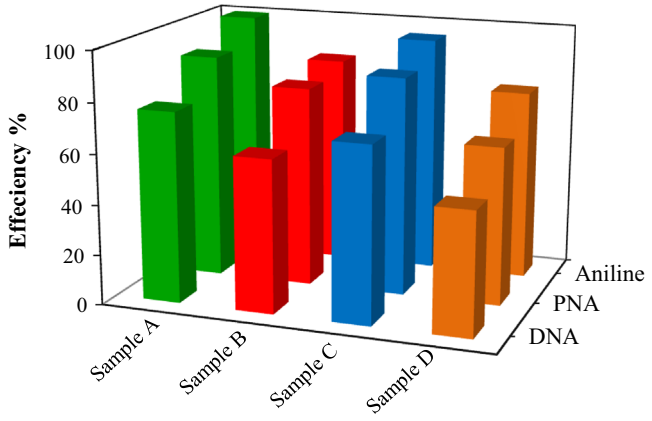


Fig. 7. Comparison of degradation efficiencies between aniline compounds for different samples as catalyst.

ratio between 250–350 nm and the lower band gap corresponding to more photon harvesting and photo-responsive. The specific surface area is of primary importance in heterogeneous catalysis because it is directly related to the efficiency of a catalyst through the organic adsorption capacity. The higher surface area of sample A favored its catalytic activity due to the adsorption of more aniline molecules on the surface. However, the surface areas and the catalytic activity data for all samples were not in the same order demonstrating that there are other more important factors that govern activity.

### 3.5. Effect of the substituents on degradability

It can be observed from Table 2 and Fig. 7 that the substituted anilines degraded slower than aniline and the photodegradation efficiencies are as follows: aniline > P-NA > DNA. The electronic character (electro-withdrawing or electro-donor) and the position of substitution on phenyl ring may affect the rate of degradation. The structure of aniline-derivatives, the strong acceptor group ($–NO_2$), makes electron density lower on the phenyl ring. Hydroxyl radical has a strong electrophilic character [66–68], it attacks easily to the aromatic ring with higher electron density. It seems that aromatic ring opening after •OH radical attack and hydroxylated radical formation is favored when no acceptor group substitute on the aromatic ring. There are no clear reports so far to take into account structure–reactivity relationships; a possible reason for the lack of structure–reactivity relationship may be due to the different interactions of the substituent with the catalyst surface and the electron density change on the phenyl ring.

### 3.6. Effect of pH

Photodegradation experiments were carried out at pH values of 4, 7 and 10, respectively. Table 2 shows the typical results of degradation of aniline compounds at various solution pH under 120 min UV irradiation. We can observe two types of behavior. The degradation of aniline is more favored at higher pH compared to its nitro-derivatives. The pH dependence is one of the most relevant parameters in the photocatalytic process because it may affect the catalyst surface properties and the substrate structure, changing the photocatalytic degradation. All these effects can be attributed to the extent of phenolic compound ionization in aqueous solution that influences the degradation rate due to different the interaction and affinity between semiconductor surface and organic compounds as the solution pH varies.

In the acidic pH, minimization of electron–hole recombination and on the other hand, higher availability of hydroxyl ions at basic pH reacting with the holes to form hydroxyl radicals are important factors for the enhanced degradation at both acidic and basic media. However, the interpretation of pH effect on the photocatalytic processes is very difficult because of its multiple roles on electrostatic interactions between the semiconductor surface, solvent molecules, substrate and charged radicals formed during the reaction process, etc.

## 4. Conclusion

Tunable synthesis of $SnO_2$ nanostructures has been achieved via hydrothermal method without using any surfactants. The morphologies of rod, spherical and flower can be obtained by the adjustment of reaction time and temperature. The samples photocatalytic activities were studied toward aniline compounds degradation. Flower-shape $SnO_2$ showed higher activities indicating important role of morphology on the photodegradation efficiency. It is also observed that the electro-withdrawing ($–NO_2$) group and its position on phenyl ring affected the rate of degradation. Further, the degradation of aniline is more favored at higher pH compared to its nitro-derivatives which are degraded at acidic media.

## Acknowledgment

The authors are grateful for the financial support provided by Islamic Azad University, Shahreza branch.

## References


[1] B.K.H. Yen, N.E. Stott, K.F. Jensen, M.G. Bawendi, A continuous-flow microcapillary reactor for the preparation of a size series of CdSe nanocrystals, Advanced Materials 15 (2003) 1858–1862.

[2] T. Hyeon, Chemical synthesis of magnetic nanoparticles, Chemical Communications 8 (2003) 927–934.

[3] W.S. Seo, J.H. Shim, S.J. Oh, E.K. Lee, N.H. Hur, J.T. Park, Phase- and size- controlled synthesis of hexagonal and cubic CoO nanocrystals, Journal of American Chemical Society 127 (2005) 6188–6189.

[4] X.J. Zhang, Q.R. Zhao, Y.P. Tian, Y. Xie, Fabrication of CdS micropatterns: effects of intermolecular hydrogen bonding and decreasing capping ligand, Crystal Growth and Design 4 (2004) 355–359.

[5] C. Tatsuyama, S. Ichimura, Electrical and optical properties of gase-$SnO_2$ heterojunctions, Japanese Journal of Applied Physics 15 (1976) 843–847.

[6] W. Dazhi, W. Shulin, C. Jun, Z. Suyuan, L. Fangqing, Microstructure of $SnO_2$, Physical Review B 49 (1994) 14282–14285.

[7] P.G. Harrison, M.J. Willett, The mechanism of operation of tin (IV) oxide carbon monoxide sensors, Nature 332 (1988) 337–339.

[8] Y.S. He, J.C. Campbell, R.C. Murphy, M.F. Arendt, J.S. Swinnea, Electrical and optical characterization of Sb:$SnO_2$, Journal of Materials Research 8 (1993) 3131–3134.

[9] S. Semancik, T.B. Fryberger, Model studies of $SnO_2$-based gas sensors: vacancy defects and Pd additive effects, Sensors and Actuators B 1 (1990) 97–102.

[10] X.G. Han, M.S. Jin, S.F. Xie, Q. Kuang, Z.Y. Jiang, Y.Q. Jiang, Z. X. Xie, L.S. Zheng, Synthesis of tin dioxide octahedral nanoparticles with exposed high-energy {221} facets and enhanced gas-sensing properties, Angewandte Chemie International Edition 48 (2009) 9180–9183.

[11] H.G. Yang, H.C. Zeng, Self-construction of hollow $SnO_2$ octahedra based on two-dimensional aggregation of nanocrystallites, Angewandte Chemie International Edition 43 (2004) 5930–5933.

[12] L. Vayssieres, M. Graetzel, Highly ordered $SnO_2$ nanorod arrays from controlled aqueous growth, Angewandte Chemie International Edition 43 (2004) 3666–3670.

[13] B. Cheng, J.M. Russell, W.S. Shi, L. Zhang, E.T. Samulski, Large-scale, solution-phase growth of single-crystalline $SnO_2$ nanorods, Journal of American Chemical Society 126 (2004) 5972–5973.

[14] M.S. Park, G.X. Wang, Y.M. Kang, D. Wexler, S.X. Dou, H.K. Liu, Preparation and electrochemical properties of $SnO_2$ nanowires for application in lithium-ion batteries, Angewandte Chemie International Edition 46 (2006) 750–753.

[15] S. Mathur, S. Barth, H. Shen, J.C. Pyun, U. Werner, Size-dependent photo-conductance in $SnO_2$ nanowires, Small 1 (2005) 713–717.

[16] M. Law, H. Kind, B. Messer, F. Kim, P.D. Yang, Photochemical sensing of $NO_2$ with $SnO_2$ nanoribbon nanosensors at room temperature, Angewandte Chemie International Edition 41 (2002) 2405–2408.

[17] X.W. Lou, Y. Wang, C.L. Yuan, J.Y. Lee, L.A. Archer, Template-free synthesis of $SnO_2$ hollow nanostructures with high lithium storage capacity, Advanced Materials 18 (2006) 2325–2329.

[18] C. Burda, X. Chen, R. Narayanan, M.A. El-Sayed, Chemistry and properties of nanocrystals of different shapes, Chemical Review 105 (2005) 1025–1102.

[19] J.Q. Hu, X.L. Ma, N.G. Shang, Z.Y. Xie, N.B. Wong, C.S. Lee, S.T. Lee, Large-scale rapid oxidation synthesis of $SnO_2$ nanoribbons, Journal of Physical Chemistry B 106 (2002) 3823–3826.

[20] Y. Liu, J. Dong, M. Liu, Well-aligned 'nano-box-beams' of $SnO_2$, Advanced Materials 16 (2004) 353–356.

[21] J.H. Ba, J. Polleux, M. Antonietti, M. Niederberger, Nonaqueous synthesis of tin oxide nanocrystals and their assembly into ordered porous mesostructures, Advanced Materials 17 (2005) 2509–2512.

[22] S.J. Han, B.C. Jang, T. Kim, S.M. Oh, T.H. Hyeon, Simple synthesis of hollow tin dioxide microspheres and their application to lithium-ion battery anodes, Advanced Functional Materials 15 (2005) 1845–1850.

[23] E.R. Leite, I.T. Weber, E. Longo, J.A. Varela, A new method to control particle size and particle size distribution of $SnO_2$ nanoparticles for gas sensor applications, Advanced Materials 12 (2000) 965–968.

[24] G.S. Pang, S.G. Chen, Y. Koltypin, A. Zaban, S. Feng, A. Gedanken, Controlling the particles size of calcined $SnO_2$ nanocrystals, Nano Letters 1 (2001) 723–726.

[25] T.C. Yeh, K.M. Hickman, S.C. Goel, A.M. Viano, P.C. Gibbons, W. E. Buhro, Solution-liquid–solid growth of crystalline III–V semiconductors: an analogy to vapor–liquid–solid growth, Science 270 (1995) 1791–1794.

[26] Z.Q. Liu, D.H. Zhang, S. Han, C. Li, T. Tang, W. Jin, X. Liu, B. Lei, C. Zhou, Laser ablation synthesis and electron transport studies of tin oxide nanowires, Advanced Materials 15 (2003) 1754–1757.

[27] Y.L. Wang, X.C. Jiang, Y.N. Xia, A solution-phase, precursor route to polycrystalline $SnO_2$ nanowires that can be used for gas sensing under ambient conditions, Journal of the American Chemical Society 125 (2003) 16176–16177.

[28] Q.R. Zhao, Y. Gao, X. Bai, C. Wu, Y. Xie, Facile synthesis of $SnO_2$ hollow nanospheres and applications in gas sensors and electrocatalysts, European Journal of Inorganic Chemistry 2006 (2006) 1643–1648.

[29] H. Wang, J. Liang, H. Fan, B. Xi, M. Zhang, S. Xiong, Y. Zhu, Y. Qian, Synthesis and gas sensitivities of $SnO_2$ nanorods and hollow microspheres, Journal of Solid State Chemistry 181 (2008) 122–129.

[30] M.N.A. Karlsson, K. Deppert, L.S. Karlsson, M.H. Magnusson, J. O. Malm, N.S. Srinivasan, Compaction of agglomerates of aerosol nanoparticles: a compilation of experimental data, Journal of Nanoparticle Research 7 (2005) 43–49.

[31] J.H. Yen, P.W. Tasi, W.C. Chen, Y.S. Wang, Fate of anilide and aniline herbicides in plant- materials-amended soils, Journal of Environmental Science and Health B 43 (2008) 382–389.

[32] C.D. Lyons, S. Katz, R. Bartha, Persistence and mutagenic potential of herbicide-derived aniline residues in pond water, Bulletin of Environmental Contamination and Toxicology 35 (1985) 696–703.

[33] USEPA, United States Environmental Protection Agency, OPPT Chemical Fact Sheets, Aniline Fact Sheet, Support Document (CAS No. 62-53-3), December 1994.

[34] C.P. Saint, N.C. McClure, W.A. Venables, Physical map of the aromatic amine and m-toluate catabolic plasmid pTDNI in *Pseudomonas putida.* location of a unique meta-cleavage pathway, Journal of General Microbiology 136 (1990) 615–625.

[35] S.P Kamble, S.B. Sawant, J.C. Schouten, V.G. Pangarkar, Photocatalytic and photochemical degradation of aniline using concentrated solar radiation, Journal of Chemical Technology and Biotechnology 78 (2003) 865–872.

[36] T. Lopez, R. Gomez, Photocatalytic activity in the 2,4-dinitroaniline decomposition over $TiO_2$ sol-gel derived catalysts, Journal of Sol-Gel Science and Technology 22 (2001) 99–107.

[37] S. Gautam, S.P. Kamble, S.B. Sawant, V.G. Pangarkar, Photocatalytic degradation of 4-nitroaniline using solar and artificial UV radiation, Chemical Engineering Journal 110 (2005) 129–137.

[38] Y. Li, F. Wang, G. Zhou, Y. Ni, Aniline degradation by electrocatalytic oxidation, Chemosphere 53 (2003) 1229–1234.

[39] A. Oren, P. Gurevich, Y. Henis, Reduction of nitrosubstituted aromatic compounds by the halophilic anaerobic eubacteria *Haloanaerobium praevalens* and *Sporohalobacter marismortui*, Applied Environmental Microbiology 57 (1991) 3367–3370.

[40] J.C. Spain, Biodegradation of nitroaromatic compounds, Annual Review of Microbiology 49 (1995) 523–555.

[41] M.A. Oturan, J. Peiroten, P. Chartrin, A.J. Acher, Complete destruction of *p*-nitrophenol in aqueous medium by electro-Fenton method, Environmental Science Technology 34 (2000) 3474–3479.

[42] A. Saupe, High-rate biodegradation of 3- and 4-nitroaniline, Chemosphere 39 (1999) 2325–2346.

[43] Z. Qing-rui, Controllable synthesis and catalytic activity of $SnO_2$ nanostructures at room temperature, Transactions of Nonferrous Metals Society of China 19 (2009) 1227–1231.

[44] H. Zhang, C. Hu, X. He, L. Hong, G. Du, Y. Zhang, Pt support of multidimensional active sites and radial channels formed by $SnO_2$ flower-like crystals for methanol and ethanol oxidation, Journal of Power Sources 196 (2011) 4499–4505.

[45] H. Zhang, C. Hu, S. Chen, K. Zhang, X. Wang, Synthesis of $SnO_2$ nanostructures and their application for hydrogen evolution reaction, Catalysis Letters 142 (2012) 809–815.
[46] A. Castro-Grijalba, J. Urresta, A. Ramirez, J. Barrault, Preparation and characterization of catalysts based on cassiterite ($SnO_2$) and its application in hydrogenation of methyl esters, Journal of the Argentine Chemical Society 98 (2011) 48–59.
[47] N. Talebian, M.R. Nilforoushan, R. Ramazan Ghasem, Enhanced photocatalytic activities of ZnO thin films: a comparative study of hybrid semiconductor nanomaterials, Journal of Sol-Gel Science and Technology 64 (2012) 36–46.
[48] J. Kim, J.S. Lee, M. Kang, Synthesis of nanoporous structured $SnO_2$ and its photocatalytic ability for bisphenol destruction, Bulletin of Korean Chemical Society 32 (2011) 1715–1720.
[49] S.K. Kansal, M. Singh, D. Sud, Studies on photodegradation of two commercial dyes in aqueous phase using different photocatalysts, Journal of Hazardous Materials 22 (2007) 581–590.
[50] C.F. Lin, C.H. Wu, Z.N. Onn, Degradation of 4-chlorophenol in $TiO_2$, $WO_3$, $SnO_2$, $TiO_2/WO_3$ and $TiO_2/SnO_2$ systems, Journal of Hazardous Materials 15 (2008) 1033–1039.
[51] T. An, M. Zhang, X. Wang, G. Sheng, J. Fu, Photocatalytic degradation of gaseous trichloroethene using immobilized $ZnO/SnO_2$ coupled oxide in a flow-through photocatalytic reactor, Journal of Chemical Technology and Biotechnology 80 (2005) 251–258.
[52] K. Vinodgopal, Prashant V. Kamat, Enhanced rates of photocatalytic degradation of an azo dye using $SnO_2/TiO_2$ coupled semiconductor thin films, Environmental Science and Technology 29 (1995) 841–845.
[53] H.L. Xia, H.S. Zhuang, T. Zhang, D.C. Xiao, Photocatalytic degradation of Acid Blue 62 over $CuO–SnO_2$ nanocomposite photocatalyst under simulated sunlight, Journal of Environmental Science (China) 19 (2007) 1141–1145.
[54] M. Davis, W.M. Hikal, C. Gümeci, L.J. Hope-Weeks, Aerogel nanocomposites of $ZnO–SnO_2$ as efficient photocatalysts for the degradation of rhodamine B, Catalysis Science Technology 2 (2012) 922–924.
[55] R. Ali, W.A.W. Abu Bakar, S.S. Mislan, M.A. Sharifuddin, Photodegradation of n-methyldiethanolamine over $ZnO/SnO_2$ coupled photocatalysts, Transactions C: Chemistry and Chemical Engineering 17 (2010) 124–130.
[56] A. Ignaszak, C. Teo, S. Ye, E. Gyenge, $Pt–SnO_2–Pd/C$ electrocatalyst with enhanced activity and durability for the oxygen reduction reaction at low Pt loading: the effect of carbon support type and activation, Journal of Physical Chemistry C 114 (2010) 6488–16504.
[57] M. Batzill, K. Katsiev, U. Diebold, Influence of subsurface, charged impurities on the adsorption of chlorine at $TiO_2$ (110), Surface Science 529 (2003) 295–311.
[58] V.A. Gercher, D.F. Cox, J.-M. Themlin, Oxygen-vacancy-controlled chemistry on a metal-oxide surfacemethanol dissociation and oxidation on $SnO_2$ (110), Surface Science 306 (1994) 279–293.
[59] D.F. Cox, T.B. Fryberger, S. Semancik, Oxygen vacancies and defect electronic states on the $SnO_2$ (110), Physical Review B 38 (1988) 2072–2083.
[60] J. Oviedo, M.J. Gillan, Energetics and structure of stoichiometric $SnO_2$ surfaces studied by first-principles calculations, Surface Science 463 (2000) 93–101.
[61] A. Beltran, J. Andres, E. Longo, E.R. Leite, Thermodynamic argument about $SnO_2$ nanoribbon growth, Applied Physical Lettres 83 (2003) 635–637.
[62] P.A. Mulheran, J.H. Harding, The stability of $SnO_2$ surfaces, Modelling and Simulation in Materials Science and Engineering 1 (1992) 39–43.
[63] A. Birkel, Interaction of alkaline metal cations with oxidic surfaces: effect on the morphology of $SnO_2$ nanoparticles, Langmuir 26 (2010) 3590–3595.
[64] D. Frohlich, R. Kenklies, Bandgap Assignment in $SnO_2$ by two-photon spectroscopy, Physical Review Letter 41 (1978) 1750–1751.
[65] G. Mills, Z.G. Li, D. Meisel, Photochemistry and spectroscopy of colloidal arsenic sesquisulfide, Journal of Physical Chemistry 92 (1988) 822–828.
[66] S. Gautam, S.P. Kamble, S.B. Sawant, V.G. Pangarkar, Photocatalytic degradation of 4-nitroaniline using solar and artificial UV radiation, Chemical Engineering Journal 110 (2005) 129–137.
[67] V. Brezova, M. Ceppan, M. Breza, E. Brandsteterova, L. Lapcik, Photocatalytic hydroxylation of benzoic acid in aqueous titanium dioxide suspension, Journal of Photochemistry and Photobiology A 59 (1991) 385–391.
[68] M.K. Eberhardt, M. Yoshida, Radiation-induced hemolytic aromatic substitution. I. Hydroxylation of nitrobenzene, chlorobenzene, and toluene, Journal of Physical Chemistry 77 (1973) 589–597.